Hydration Dependence of Chain Dynamics and Local Diffusion in L-α-Dipalmitoylphosphtidylcholine Multilayers Studied by Incoherent Quasi-Elastic Neutron Scattering

S. König,* T. M. Bayerl,* G. Coddens,‡ D. Richter,§ and E. Sackmann*
*Physik-Department E22, TU München, D-85747 Garching, Germany, ‡Laboratoire Léon Brillouin, CEA Saclay, F-91191 Gif-sur-Yvette, France, and §Forschungszentrum Jülich, IFF, D-52425 Jülich, Germany

ABSTRACT Incoherent quasi-elastic neutron scattering is applied to study the local diffusion and chain dynamics of L-α-dipalmitoylphosphatidylcholine molecules in oriented model membranes. Different motions are distinguished by changing the hydration of the multilayers as well as by measuring below and above the gel-to-liquid crystalline phase transition. The time range of the utilized time-of-flight spectrometer permits to observe two types of motion to be observed more closely: chain defect motions and the local diffusion of the whole molecule in its solvation cage. Oriented lipid membranes are a useful system for the observation of chain defects, as they can be macroscopically oriented, in contrast to most polymers. As a representative model for a chain defect a kink is chosen and the corresponding scattering functions are derived. The kink motion can explain the entire dynamics seen in the gel phase, and the lifetime of such a defect was found to be 10–15 ps, in good agreement with theoretical predictions. On the other hand the dynamics in the liquid crystalline phase cannot be explained even by a superposition of several kinks and thus requires the consideration of an additional motion: the local diffusion of the molecule in its solvation cage. The size of the solvation cage is increasing with multilayer hydration and reduced temperature. Particularly interesting in view of recent discussions about the origin of the short-range repulsive forces between membranes is the experimental finding of an out-of-plane motion with an amplitude of 1–1.5 Å, which cannot be explained by the undulation of the whole membrane.

INTRODUCTION

While the structure of lipids and lipid mixtures has been the subject of a large number of publications (e.g., Tardieu and Luzzati, 1973; Hauser et al., 1981), the lipid dynamics has been much less studied. Long-range lateral diffusion as a relatively slow motion has been investigated by fluorescence techniques (Vaz et al. 1985), NMR relaxation methods can give information on slow motions as well as on motions on the time scale of nanoseconds (Dolainsky et al., 1993; Koechy and Bayeri, 1993), and IR spectroscopy is probing motion in the picosecond regime (Mendelssohn et al., 1989; Casal and McElhaney, 1990). However, no explicit information on lipid molecular motion can be derived from IR measurements because of the lack of theoretical background. Moreover, the dynamical windows of these techniques leave large gaps, where little or nothing is known so far. Incoherent quasi-elastic neutron scattering, and in particular the time-of-flight method applied here, can probe motions on the time scale 10^{-11}–10^{-13} s and thus helps to close the gap between NMR and Raman measurements. Expected motions in this regime are chain defects, fast head-group motions, and the local diffusion of the molecule in its solvation cage. The head-group motion cannot be distinguished in our experiments, as we used protonated lipids and the scattering of the chain only amounts to 77% of the total scattering.

Time of flight spectroscopy has already proven to be a useful technique in the study of soft materials (polymers, liquid crystals (e.g., Bée, 1988)) and is by now also applied to biological problems (e.g., (Smith, 1991; Tabony and Perly, 1990). The possibility of probing energy and momentum transfer simultaneously is a unique feature, and one thus obtains information on the geometry as well as on the correlation times of motions in the same measurement. Further advantages of incoherent quasi-elastic neutron scattering compared with the above-mentioned techniques include the following: motions of part of the molecule can be screened by selective deuteration, the anisotropy of motions can be resolved by using oriented samples and choosing the angle between sample and neutron beam accordingly, and different values of the momentum transfer can be measured simultaneously.

The dynamics of lipids in multilayers is strongly influenced by their packing density, as has already been seen, e.g., with lateral diffusion (Galla et al., 1979; Peters and Beck, 1983; Vaz et al., 1985). A convenient way to change the packing density is the variation of the degree of hydration of the multilayers (Levine et al., 1968). In this paper we present measurements for hydrations between 8 and 20 wt. % of water, corresponding to 3–10 molecules of water per lipid molecule.

Received for publication 1 August 1994 and in final form 23 December 1994.
Address reprint requests to Dr. Sabine König, Centre de Recherche Paul Pascal; Avenue de Dr. Schweitzer, F-33600 Pessac, France. Tel.: 33–56845608; FAX: 33–56845600; E-mail: Koenig@crpp.u-bordeaux.fr.
Dr. König's current address: Centre de Recherche Paul Pascal, Avenue de Dr. Schweitzer, F-33600 Pessac, France.

0006-3495/95/05/01/10 $2.00

In a previous study of incoherent quasi-elastic neutron scattering (König et al., 1992) the local and chain defect motion were interpreted by using the q dependence of the elastic incoherent structure factor (EISF). While the EISF is a measure of the order of the chain and thus an average quantity, the temporal dependence of a process can be derived by simultaneously fitting all spectra to a model function. The latter approach is chosen in this paper, and the structure factor for the models is calculated.

Protrusion forces, as put forward by Israelachvilli and Wennerstroem (1992), require an out-of-plane motion of the whole molecule. These motions lie within the time scale of the presented measurement, and we are thus able to give an experimental value for the protrusion parameters.

MATERIALS AND METHODS

Sample preparation

For all measurements L-α-dipalmitoylphosphtidylcholine (DPPC) was used, which was purchased from Avanti Polar Lipids, Alabaster, AL. The lipid was used without further purification; the purity was checked using differential scanning calorimetry by measuring the half-width at half-maximum of the main phase transition. The lipid was hydrated with deuterated water (Sigma Chemie GmbH, Deisenhofen, Germany). For the preparation of ordered multilayers undoped silicon wafers were used as substrates (Virginia Semiconductors, Inc., Fredericksburg, Virginia), which were etched to a thickness of 150 μm and polished on both sides. Standard air-tight sample holders, made of aluminium, were used for the neutron scattering experiments.

The preparation of highly ordered multilayers has been described in detail elsewhere (König et al., 1992). The hydration of the multilayers was varied during preparation by equilibrating them against different saturated salt solutions at elevated temperatures (Levine et al., 1968). Because of the sensitivity of this procedure to preparation details, the final water content of the sample can be predicted only to about ±1 wt. %. Therefore all samples used for quasi-elastic measurements were characterized by other methods (see the following subsection). There is a swelling limit for lipids hydrated from air humidity, which is ~20 wt. % of water for DPPC. To obtain a sample with higher water content, the pure DPPC was replaced by a mixture DPPC/5 mol. % Dipalmitoyl phosphatidylglycerol. The latter carries a negative excess charge in its head group.

The advantage of ordered multilayers is the ability to choose a scattering geometry that allows motion parallel and perpendicular to the membrane normal to be distinguished. The standard geometry for this purpose is to orient the sample in such a way that the membrane normal and the incident neutron beam enclose an angle of 45° (motion parallel to the membrane normal) or 135° (motion perpendicular to the membrane normal) (Pfeiffer et al., 1989).

Sample characterization

The degree of water hydration can be determined in one of two ways:

(1) The phase diagram of DPPC/water as a function of hydration is well known (Jürgens, 1981; Sackmann, 1983), and one salient feature is the increase of the main transition temperature T_c from the gel to the liquid crystalline phase with decreasing hydration. Thus T_c can be taken as a sensitive measure of the degree of hydration. In time-of-flight experiments the elastic intensity (i.e., the sum of intensities in the channels corresponding to purely elastic scattering) as a function of temperature decreases remarkably faster in the vicinity of the transition temperature than in one of the two phases. This effect is used to determine the transition temperature of the sealed samples.

If the hydration is below saturation, the transition broadens and stretches over a coexistence region (Jürgens, 1981). In that case the transition temperatures stated in the text are the midpoint of the observed transition region.

(2) A second measure of the degree of hydration was the determination of the repeat distance of the multilayers. This was done using the triple-axis spectrometer F3 at the research reactor of the TU Munich. The advantages of this diffraction scan are that it averages over the whole sample and that also a "rocking curve" measurement (König et al., 1992) can be performed to determine the mosaicity of the sample. The values of repeat distance and mosaic spread are given in Table 1. The variation of the repeat distance between 56.9 and 59 Å is in good agreement with previous measurements (Torbet and Wilkins, 1976); the fairly large error in d_r is due to having observed only two to three diffraction orders. This error is also the reason that the same value of d_r for the samples with 18 and 8 wt. % of water has been found. The variation observed by other authors is within our error.

Method

The availability of high-resolution spectrometers in quasi-elastic neutron scattering has lead to a wide range of applications also for the study of the dynamics of soft materials (e.g., Bée, 1988). However, despite the numerous advantages of the method, its potential for applications in membrane biophysics has not been fully appreciated yet. We will thus recall its main features.

Because the neutron is a spin 1/2 particle, a neutron can be scattered with or without spin flip (see any textbook on the principles of neutron scattering, e.g., Lovesey, 1984). Thus two scattering cross-sections have to be distinguished, the coherent and the incoherent scattering cross-section. Coherent scattering probes the *pair correlation* function between different scatterers in a sample and can thus give information about structural properties as well as correlated dynamics such as undulations. It is the analog to the familiar scattering cross section in x rays. Incoherent scattering has no analog in x rays (it arises from the spin interaction of neutron and sample) and probes the *autocorrelation* function of the scattering particles. It can give information on diffusive motions as well as on the density of states of correlated motions. The distinction of these two types of scattering is simply made by choosing a "convenient" scatterer; in the case of biological materials the proton is a strongly incoherent scatterer. The deuteron scatters mainly coherently, but again much more weekly than the incoherent scattering of the proton, and therefore deuteration is a means to mask (parts of) molecules in incoherent scattering experiments (such as the water in the experiments described below).

All experiments described in this paper were performed at time-of-flight spectrometers (mainly MIBEMOL at LLB, Saclay, but also IN5 at ILL, Grenoble). Time of flight describes the method of analyzing the energy of the scattered neutron: it is done simply by measuring the neutron's flight time from sample to detector (e.g., Bée, 1988). The energy resolution in the experiments (full width at half-maximum) was 50 μeV (MIBEMOL) and 63 μeV (IN5); i.e., motions on the time scale of 10^{-11} s can be resolved. The accessible q range is 0.2–1.6^{-1} Å^{-1} at λ = 7.5 Å and detectors spanning an angle of 140° (e.g., MIBEMOL).

The resolution of the spectrometer is determined by using a vanadium sample, which is an elastic incoherent scatterer. The resolution function is a triangle in first approximation, and, as the quasi-elastic broadening is expected to be Lorentzian, a distinction between elastic and quasi-elastic contributions is possible, even if the line width of the Lorentzian is quite small.

TABLE 1 Repeat distance d_r and mosaic spread of the samples used, as determined on the triple-axis spectrometer F3 (research reactor of the TU Munich, Germany)

Sample	d_r	Mosaic spread	T_c
DPPC 18 wt. % water	59.0 ± 0.5Å	2°	45°C
DPPC 8 wt. % water	59.0 ± 0.8Å	5°	70°C
DPPC 5 wt. % water	56.9 ± 0.2Å	2°	80°C
DPPC + 5 mol. % DPPG	63.5 ± 2.0Å	10°	41°C

The values were taken at room temperature. T_c is the midpoint of the transition as determined by a decrease in the elastic scattering.

Data evaluation

The data evaluation is usually performed in two steps: In the first step an elastic line plus one or two Lorentzians are fitted to each spectrum, i.e., to the intensity as a function of energy for each angle. The relative intensity of the elastic line is the EISF (or $A_0(q)$), and its q dependence is a valuable piece of information in determining the geometry of the motion.

The theoretical basis for this procedure is the possibility of expanding the scattering functions of all motions considered into a series of Lorentzian lines and taking only the leading terms of this series. The theoretical fitting function can be expressed as

$$S_{inc}(q, \omega) = S_{inst} \otimes Ie^{-DWF}\{A_0(q)\,\delta(\omega) + A_1(q)\,L_1(\Gamma_1, \omega) + A_2(q)\,L_2(\Gamma 2,\omega)\} + BG, \quad (1)$$

where S_{inst} is the resolution function, $\otimes$ is convolution, L_i are Lorentzian lines of width (HWHM) Γ_i, $A_i(q)$ is the corresponding amplitude, I is the absolute intensity, DWF is the Debye-Waller factor, and BG is the possible background.

As in previous measurements (König et al., 1992) an elastic line plus two Lorentzian lines were required to fit our spectra. The broader of the two Lorentzian lines was adjusted to have a constant width for all q (as predicted by the model of an overdamped oscillator); however, allowing this width to change did not change the width of the narrow line appreciably. This independence of the two line widths is due to the large difference in their values (broad line, ≈2 meV; narrow line, ≈30 μeV).

As the main focus of this paper is on the discussion of the slower motions, i.e., on the narrow Lorentzian line, it should be mentioned only briefly that the mean square amplitudes found for the fast motion (broad line) are linear in temperature, as expected for an overdamped oscillator. Thus some kind of fast relaxing mode is most likely for this motion.

The second step in data evaluation is to find a model for the motion that is compatible with the observed q dependences of EISF and line width. The model function $S(q, \omega)$ convoluted with the resolution function is then fitted simultaneously to all spectra. The free parameters are the model parameters such as transition rates or jump lengths (see also the following section of this paper).

If parameters for in- and out-of-plane motion are to be fitted and measurements at 45° and 135° orientation are available, the fitting procedure is an iterative process between the two sets of data. The spectra for the 45° (135°) orientation are not totally independent of the parameters for the motion perpendicular (parallel) to the membrane normal **n**; thus, while fitting the data of the 45° (motion parallel **n**) or 135° (motion perpendicular **n**) orientation, the parameters for the data of the other orientation were kept constant. Then the other orientation was treated, and again the first one. This was done until the parameters for each direction did not change any more within error.

The data presented in this paper were always analyzed by both procedures; the figures showing EISF and line width should not lead to the assumption that the second step of the data treatment was neglected. However, most effects are more conveniently shown in EISF and line width presentations.

MODELS FOR CHAIN DEFECT AND LOCAL DIFFUSION MOTION

The dynamics of hydrocarbon chains has been described in terms of defect motion by Träuble (1971) and has been indirectly measured by NMR or FTIR (Schindler and Seelig, 1975, Casal and McElhaney, 1990). Other approaches to describe the dynamics of membranes include the Pink 10 state model (Caillé et al., 1980) and the mattress model (Mouritsen and Bloom, 1993).

In polymers different types of defects are described: simple gauche defects, kinks, jogs, etc. (see, e.g., Helfand and Skolnick, 1982). For the following model calculations, only kink defects (using the trans-gauche notation familiar to several readers, a kink is a $g^+_- t\, g^-_+$ defect; see also the Appendix) will be considered, although they are probably not the most common defect. However, this approach can be justified as follows: for the dynamics of the system, i.e., the line widths observed, the rates with which defects transform into each other are the dominating parameters. These rates should be similar for different types of defect. The geometry of the defect, which is comparatively simple for a kink defect, comes into play for the amplitude of each Lorentzian line. However, because of inequivalent proton positions an average over several different lengths has to be taken in all defect models. Therefore the resulting scattering function depends not only on the type of defect but also on the averaging process (dimension and weight of each length involved).

The following section presents model calculations for the scattering function resulting from the motion of a kink defect. For readers not familiar with this type of calculation a short introduction into the formalism is given.

MASTER EQUATION FORMALISM

To describe the dynamics of a system, which can assume different states, a time-dependent probability vector $P_n(t)$ is introduced. $P_n(t)$ describes the probability of finding the system in state Φ_n at time t. The state Φ_n is a description of the state of the whole chain; e.g., if a chain has L bonds and each of these bonds can be in l configurations, there are L^l different states Φ_n for the chain. The dynamics can then be described by the master equation (Springer, 1972; Richter and Ewen, 1978; Bahar and Erman, 1987):

$$\frac{dP_n(t)}{dt} = \sum_{m=0}^{N-1} A_{mn} P_m(t), \quad (2)$$

where A_{mn} is the $N \times N$ transition matrix. The elements of A_{mn} are the probabilities per second that the system undergoes a transition from state Φ_m to state Φ_n. Equation 2 can be solved formally by the ansatz

$$P_n(t) = \sum_{k=0}^{N-1} E_n^k \exp(-\lambda_k t)\, P_n(t=0), \quad (3)$$

where λ_k are the eigenvalues and E_n^k the eigenvectors of A_{mn} $P_n(t = 0)$ is the equilibrium distribution of states.

Each eigenvalue represents a characteristic relaxation time of the system. If the motion is restricted in space, zero is always one of the eigenvalues.

The self-correlation function can be deduced from Eq. 3 by performing the thermal average (Richter and Ewen, 1978)

$G_s(\mathbf{r}, t)$

$$= \sum_{k=0}^{N-1} \sum_{n,m=0}^{N-1} \frac{1}{N} E_n^k E_m^k \exp(-\lambda_k t)\delta(\mathbf{r} - (\mathbf{r}_n - \mathbf{r}_m)). \quad (4)$$

Fourier transformation in space and time leads to the incoherent scattering function

$$S_{inc}(\mathbf{q}, \omega) = \int d^3\mathbf{r} \int dt G_s(\mathbf{r}, t). \quad (5)$$

which is proportional to the measured quantity, the double differential scattering cross section (Springer, 1972).

Kink diffusion

The dynamic structure factor for the kink diffusion model can be calculated in analogy to the problem of a proton diffusing along a linear chain (Richter and Ewen, 1978); however, here it is a defect and not a particle that diffuses. The number of Lorentzian lines and their widths is dependent only on the number of sites available. But the amplitude of each individual line depends on the geometry of the motion. The geometry of the chain and the jump lengths of the protons involved in kink motion are presented in the appendix. It is important to note that there are always several inequivalent protons, and thus several lengths, involved in the motion of a defect (see the Appendix for the schematic drawing of the chain geometry considered here).

Assigning a number to each possible position of a kink along the chain, a kink situated at a site with an even (odd) number can only diffuse to another even (odd) number for geometrical reasons. Thus the matrix for a chain with, e.g., 14 possible kink positions decomposes into two identical 7 $\times$ 7 matrices. With the assumption that a kink can only diffuse to next-neighbour positions, this matrix has the form

$$A_{mn} = r_f \begin{Bmatrix} -1 & 1 & 0 & \dots & \dots \\ 1 & -2 & 1 & 0 & \dots \\ \dots & \dots & \dots & \dots & \dots \\ \dots & 0 & 1 & -2 & 1 \\ \dots & \dots & 0 & 1 & -1 \end{Bmatrix} \quad (6)$$

where r_f is the transition rate between neighboring kinks.

The eigenvalues and eigenvectors of this ($N \times N$) matrix are already known (Richter and Ewen, 1978):

$$\lambda_i = 2r_f\left(1 - \cos\frac{i\pi}{N}\right), \qquad i = 0, \dots, N-1,$$

$$E_n^0 = \frac{1}{\sqrt{N}},$$

$$E_n^i = \sqrt{\frac{2}{N}} \cos\left(\frac{2n+1}{2}\frac{i\pi}{N}\right). \quad (7)$$

The scattering function is derived as

$$S_{inc}(\mathbf{q}, \omega) = A_0(q)\,\delta(\omega) + \sum_{i=1}^{N-1} A_i(q)\,L_i(\lambda_i, \omega),$$

with

$$A_0(q) = \frac{1}{M}\left\{1 + \sum_{n=1}^{M-1}\sum_{m=0}^{n-1}\frac{1}{M^2}(N - 2 + 2\cos(\mathbf{qd}_1) + 2\cos(\mathbf{qd}_2) - 2|n-m| + 2|n-m-1|\cos(\mathbf{qd}_3))\right\},$$

$$A_i(q) = \frac{1}{MN}\left\{\sum_{n=0}^{M-1}\cos^2\left(\frac{2n+1}{2}\frac{i\pi}{M}\right) + \sum_{n=1}^{M-1}\sum_{m=0}^{n-1}\left(\frac{1}{M}\cos\left(\frac{2n+1}{2}\frac{i\pi}{M}\right)\cos\left(\frac{2m+1}{2}\frac{i\pi}{M}\right)\right)(N - 2 + 2\cos(\mathbf{qd}_1)\right.$$

$$\left. + 2\cos(\mathbf{qd}_2) - 2|n-m| + 2|n-m-1|\cos(\mathbf{qd}_3))\right\}. \quad (8)$$

$M = N/2$, N is the number of sites, in this case taken to be 14, and the jump lengths d_1, d_2, and d_3 are explained in the appendix.

So far we have not considered that there are only two well-defined directions: the membrane normal and the plane of the membrane. Thus we have to average all the terms with $\mathbf{qd}_i$ over the plane of the membrane. This leads to (Barnes, 1973)

$$\cos(qd) \rightarrow \cos(\mathbf{q}_\parallel d\cos\Theta)\,J_0(q_\perp d\sin\Theta).$$

For brevity the notation cos(**qd**) will be kept, but for all figures shown and data analysis performed the average has been taken.

Fig. 1 *a*) shows the EISF for this model for both orientations of the sample with respect to the neutron beam (β) that are used in the experiment. Θ is the angle between the membrane normal and the jump direction (see the Appendix) and was varied to explore the influence of, e.g., chain tilt. In Fig. 1 *b*) the EISF and all amplitudes $A_i(q)$ are shown. It is interesting to note that all $A_i(q)$ have their maxima at the same q value, in contrast to the case of a proton diffusing along a linear chain. This can be explained by appreciating that the diffusion of a proton along a chain over N sites

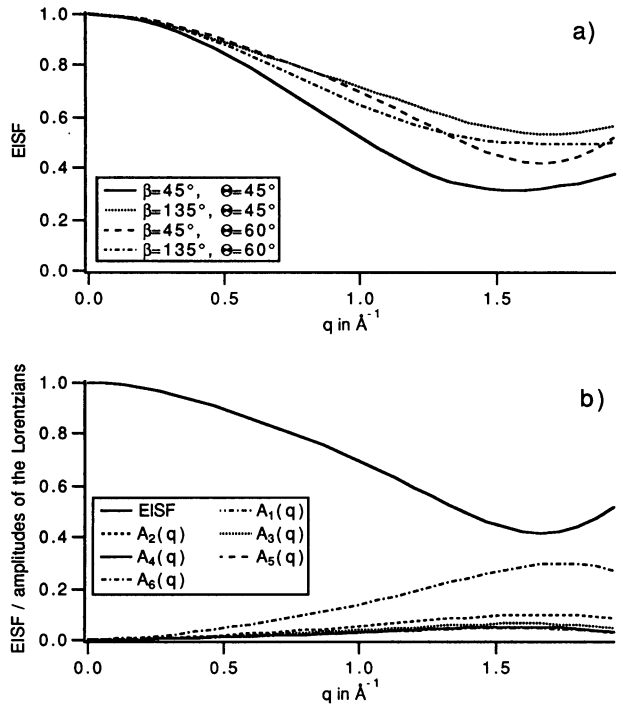

FIGURE 1 (*a*) q dependence of the EISF for the model of kink diffusion shown for different angles between membrane normal and neutron beam (β) or membrane normal and the axis of motion (Θ). (*b*) EISF and all amplitudes A_i (q), as defined in Eq. 8, for the condition $\beta = 45°$, $\Theta = 60°$.

corresponds to a diffusion length of N times the next-neighbor distance. If a kink diffuses over N sites, however, the protons attached to the chain do not jump a greater distance; there are just more protons involved in the process.

Stochastic kinks

In lipid bilayers, the model of kink diffusion is supposed to be valid only for ordered phases such as the gel phase but not in disordered phases such as the liquid crystalline phase. In molecular dynamics simulations in the L_α-phase the dominating process is not diffusion of the defect to the neighboring site but rather a stochastic appearance and disappearance of defects at random sites (S. J. Marrinck, University of Groningen, The Netherlands, personal communication, 1993). To calculate the dynamic structure factor of this model, the appropriate transition matrix is generated and is of the following form:

$$\begin{bmatrix} t & K_1^+ & K_2^+ & K_3^+ & \dots & K_1^- & K_2^- & K_3^- & \dots \\ -24r_1 & r_2 & r_2 & r_2 & \dots & r_2 & r_2 & r_2 & \dots \\ r_1 & -r_2 & 0 & 0 & \dots & \dots & \dots & \dots & \dots \\ r_1 & 0 & -r_2 & 0 & \dots & \dots & \dots & \dots & \dots \\ r_1 & 0 & 0 & -r_2 & \dots & \dots & \dots & \dots & \dots \\ \dots & \dots & \dots & \dots & \dots & \dots & \dots & \dots & \dots \\ r_1 & 0 & \dots & \dots & \dots & -r_2 & 0 & 0 & \dots \\ r_1 & 0 & \dots & \dots & \dots & 0 & -r_2 & 0 & \dots \\ r_1 & 0 & \dots & \dots & \dots & \dots & 0 & -r_2 & \dots \\ \dots & \dots & \dots & \dots & \dots & \dots & \dots & \dots & \dots \end{bmatrix},$$

where t is an all-*trans* configurations, $K_i^{+,-}$ is a kink in position i (the + sign corresponds to a $g^+t\,g^-$ defect, the − sign to $g^-t\,g^+$), r_1 is the transition rate from $K^{+,-}$ to t, and r_2 is the transition rate from t to $K^{+,-}$.

This matrix is another special case: a defect does not diffuse from one site to another but is generated at one site; the chain goes back into the all-trans conformation and the defect can be generated at a different site.

The eigenvalues of this matrix are easily evaluated to be $\lambda_0 = 0$, $\lambda_1 = -r_2$, $\lambda_2 = -\{r_2 + 24r_1\} = -24r_1\,(1 + \rho) = -r_2\,\{1 + 1/\rho\}$, $\lambda_3 - \lambda_{23} = \lambda_1$. ρ is defined as $r_2/24r_1$ and is a measure for the average number of kinks per chain. The model allows a maximum of one kink per chain; however, as there can be chains with no kink defect, the average number of kinks per chain lies between 0 (corresponding to $\rho = \infty$) and 1 ($\rho = 0$).

The probability that the system is in the all-*trans* configuration is $\rho/(1 + \rho)$, that it is in any configuration with one kink is $1/(1 + \rho)$, and that it is in a configuration with a specific kink is $1/24(1 + \rho)$. Thus there are only three different eigenvalues and thus only three Lorentzians in the sum [Eq. (1)] (to avoid complications in verbalizing the formulas we take the δ function as a Lorentzian of width zero), in contrast to the model of kink diffusion with seven different eigenvalues.

The calculation of the weight of each Lorentzian is performed using the algebraic program REDUCE and leads to the following functions:

$$A_0(q) = \frac{1}{(1+\rho)^2}\left\{\rho^2 + \frac{13}{15}\rho + \frac{1417}{2160} + \cos(\mathbf{q}\mathbf{d}_1)\left[\frac{2}{15}\rho + \frac{53}{720}\right] + \cos(\mathbf{q}\mathbf{d}_2)\left[\frac{2}{15}\rho + \frac{251}{4320}\right] + \cos(\mathbf{q}\mathbf{d}_3)\left[\frac{13}{15}\rho + \frac{917}{4320}\right]\right\},$$

$$A_1(q) = \frac{1}{1+\rho}\left\{\frac{743}{2160} - \frac{53}{720}\cos(\mathbf{q}\mathbf{d}_1) - \frac{251}{4320}\cos(\mathbf{q}\mathbf{d}_2) - \frac{917}{4320}\cos(\mathbf{q}\mathbf{d}_3)\right\},$$

$$A_2(q) = \frac{\rho}{(1+\rho)^2}\left\{\frac{341}{432} - \frac{43}{720}\cos(\mathbf{q}\mathbf{d}_1) - \frac{65}{864}\cos(\mathbf{q}\mathbf{d}_2) - \frac{2827}{4320}\cos(\mathbf{q}\mathbf{d}_3)\right\}. \quad (9)$$

In Fig. 2 the results of the stochastic kink calculation are presented. The angle Θ was always chosen to be 45°; a variation leads to results similar to those in the kink diffusion model (see Fig. 2). However, we varied the number of kinks per chain instead, or, in other words, we

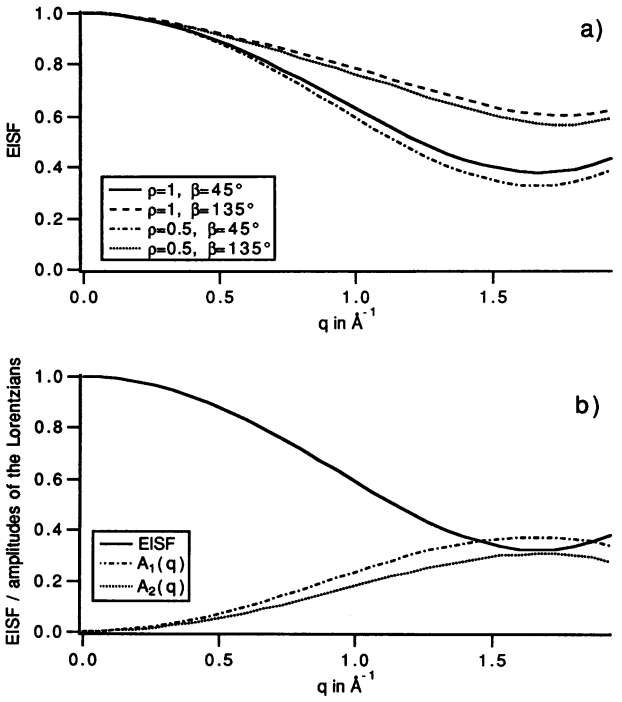

FIGURE 2 (*a*) q dependence of the EISF for the model of stochastic kinks. Again both orientations ($\beta = 45°$ and $\beta = 135°$) of the membrane normal with respect to the neutron beam are shown. The case $\rho = 1$ corresponds to an average number of 0.5 kink/chain; $\rho = 0.5$, to 0.67 kink/chain. (*b*) EISF and amplitudes of both inelastic lines for the case $\rho = 0.5$, $\Theta = \beta = 45°$.

considered the case that not every chain has a kink defect (expressed as a variation in ρ).

Comparison of the two models

It is interesting to compare the q dependence of the EISF for both models, which is done in Fig. 3 for the case of $\beta = \Theta = 45°$. One can see that the differences are too small to be resolved experimentally.

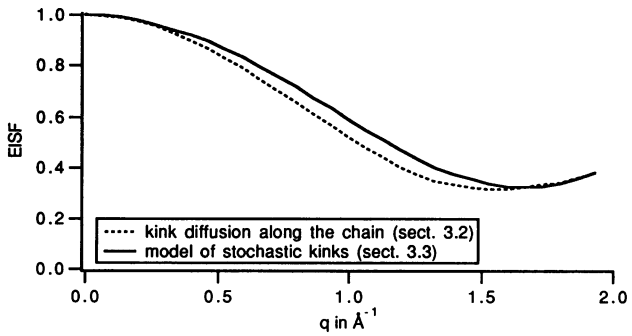

FIGURE 3 Comparison of the EISF obtained for the two kink models. In both cases the 45° orientation of the sample is shown, and $\Theta = 45°$ is taken. A value of $\rho = 0.5$ was considered for the stochastic kink model. The difference is very small, and even this difference could be removed by taking a slightly different Θ in both cases.

The two models differ, however, in the number of inelastic lines: six lines are obtained for the kink diffusion and only two for the stochastic kinks. In view of the similar q dependence of all amplitudes in the kink diffusion model as shown in Fig. 1 *b*, it does not seem feasible to distinguish these lines from an experimental point of view.

The real motion is most probably more complicated than the two models considered here, as it might involve aspects of both diffusion and spontaneous creation of defects. The calculation for the stochastic kink model (see the subsection Stochastic kinks) is quite versatile, and one could, in principle, include kink diffusion or different types of defects by choosing the appropriate matrix elements to be nonzero or by enlarging the matrix. Also, the assumption that the transition probabilities of diffusion or creation of a kink are the same at each position along the chain could be improved in that way. However, then the simple eigenvalues of the equation would be lost and the computer time will be the limiting factor of the calculation.

Considering the small differences of the calculated extremes, we believe to have given a sufficient model description for the motion of one defect in a lipid chain. For the data evaluation presented in the next subsection the stochastic kink model is chosen, as the resulting fitting routine is faster.

Diffusion in a cylinder

The model of diffusion in a cylinder will be used to describe the local diffusion of a lipid molecule in its solvation cage in the Results section. Therefore the basic facts of this model (Dianoux et al., 1982) are summarized.

The cylinder considered is of length L and radius R, and the local diffusion of the lipids is described by a diffusion coefficient $D_\parallel$ for the motion parallel and $D_\perp$ for the motion perpendicular to the cylinder axis. As the motion parallel and perpendicular to the cylinder axis is assumed to be independent, the incoherent scattering function can be written as a convolution of the two respective scattering functions:

$$S_{\text{inc}}(q, \omega) = S_\parallel(q_\parallel, \omega) \otimes S_\perp(q_\perp, \omega). \quad (10)$$

Both scattering functions, $S_\parallel(q_\parallel, \omega)$ as well as $S_\perp(q_\perp, \omega)$, are again a sum of an elastic line and inelastic (Lorentzian) lines. The corresponding expressions are quite lengthy and can be found in Dianoux et al. (1982).

RESULTS

In Fig. 4 we present EISF and line widths of all samples measured at MIBEMOL in the L_α phase (measuring temperature = 5°C above T_c; see the Methods subsection for sample characterization). For comparison the present data analysis was also applied to spectra obtained previously at IN5 (ILL, Grenoble) with a sample of $\approx$ 12 wt. % of water (see König et al., (1992) for complete data).

It can be seen that for comparable q values the EISF increases with decreasing hydration. It is well known that this corresponds to an increasing packing density. The line width,

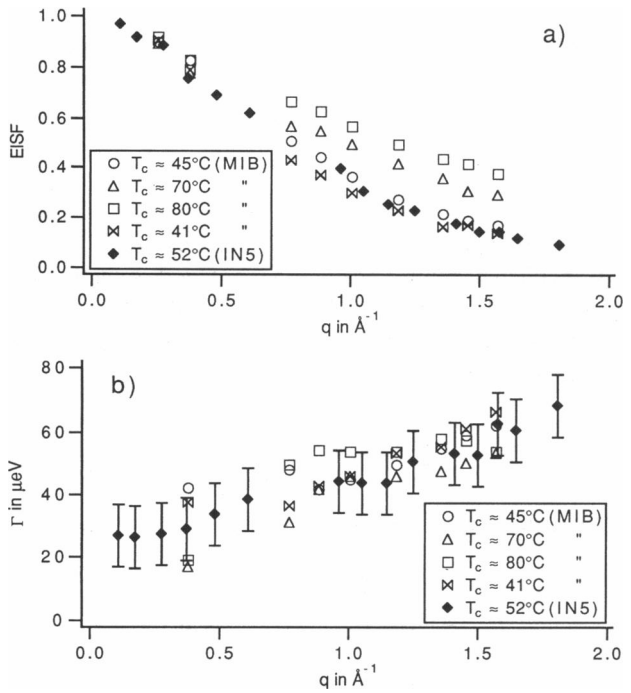

FIGURE 4 The q dependence of *a*) EISF and *b*) line widths of hydration-dependent time-of-flight measurements on DPPC multilayers is shown. The measurements were all performed in the L_α phase, at 5°C above T_c (see Table 1 for a conversion from T_c to wt. % of water). The orientation of the samples with respect to the neutron beam was 45°. For most experiments the instrument MIBEMOL (Saclay) was used; for comparison one experiment using the instrument IN5 (Grenoble) is added.

however, does not change within error. This is an indication that the correlation time of the observed dynamical process does not change with hydration, but its spatial extension increases with increasing free volume.

Similar data, measured as a function of temperature, can be found in König et al. (1992). As they were discussed only in terms of an order parameter model, we have reanalyzed them, using the same procedure as for the more recent data.

The order parameter model discussed in König et al. (1992) is sufficient for analyzing the mean chain conformation on the measured time scale. However, as it assumes the rather unphysical picture of an independent motion of each proton, it is unsuitable for treating the dynamical part of the data. Thus a model was sought that retains the good agreement between order parameter model and EISF but can additionally explain the dynamics in a physically meaningful way. The chain defect model presented in the section on Models for Chain Defect and Local Diffusion Motion fulfills this requirement. Thus, the two models cannot be distinguished in terms of fit quality, but the treatment presented in this paper is a physically sensible model for chain conformation and dynamics.

The data were now treated by the models introduced above, and significant differences for the model fitting in gel or liquid crystalline phases have been observed. In the $L_{\beta'}$ phase, the kink defect model introduced above, was sufficient to fit the spectra for all samples at all q values. No free

TABLE 2 Parameters obtained by fitting spectra obtained with DPPC in the gel phase, using the stochastic kink model

Sample	T (°C)	Kink parameter (ρ)	Number of kinks/chain	r_2 ($\times 10^{10}$ s^{-1})
IN5, $T_c \approx$ 52°C	2	4.35 ± 0.2	0.19 ± 0.02	9.4 ± 1.0
IN5, $T_c \approx$ 52°C	25	0.61	0.62	6.6
IN5, $T_c \approx$ 52°C	35	0.52	0.66	8.8
MIB, $T_c \approx$ 70°C	55	0.60	0.63	9.1

This model is sufficient to explain all gel phase data. The error given in the first line is typical for all measurements.

parameters are required to characterize the geometry of the motion, and thus the only adjustable parameters are the average number of kinks described by the number ρ and the transition rate r_2. Table 2 shows the results obtained by this procedure. While the transition rate varies only little with temperature, the number of kinks per chain increases toward its limiting value one. On the other hand, the model with one kink per chain fails in the liquid crystalline phase. Several reasons are possible: first, the number of chain defects increases in the L_α phase, as already observed with other techniques (Blume, 1993; Egberts and Berendsen, 1988). This will certainly have an effect on the scattering function, but it is unlikely that this is the major reason for the failure of our model. Even a self-convolution of our model (corresponding to two noninteracting kinks per chain) does not lead to a better fit. More importantly, the great similarity of spectra for chain deuterated and protonated molecules indicates the presence of a motion of the whole molecule (data not shown). Therefore we assume that the additional dynamical process is the diffusion of the molecule inside its solvation cage. This local diffusion should be observed whenever lateral diffusion occurs, but on a much faster time scale.

A rotation of the molecule was not considered, as the relevant time-scale, determined by NMR (Mayer et al., 1988) is not within our experimentally accessible region. Furthermore a rotational motion is not compatible with our previous data evaluation (König et al., 1992).

TABLE 3 Parameters for lipid motion in the liquid crystalline phase, described by the motion of one chain defect and a local diffusion of the whole lipid molecule in a cylinder

Sample	T (°C)	$D_\parallel$ ($\times 10^{-6}$ cm^2/s)	L (Å)	$D_\perp$ ($\times 10^{-6}$ cm^2/s)	R (Å)
IN5, $T_c \approx$ 52°C	50	1.7 ± 0.5	2.1 ± 0.3		
IN5, $T_c \approx$ 52°C	60	4.8	2.3	6.3	1.1
Mib., $T_c \approx$ 45°C	40	1.9	1.9	2.6	1.1
Mib., $T_c \approx$ 45°C	45	3.7	2.0		
Mib., $T_c \approx$ 45°C	50	5.2	3.0	6.7	1.2
Mib., $T_c \approx$ 41°C	50	6.5	3.2	7.5	1.3
Mib., $T_c \approx$ 70°C	65	1.9	1.7	3.1	1.1
Mib., $T_c \approx$ 70°C	75	4.0	2.2	7.0	1.2
Mib., $T_c \approx$ 80°C	85	3.1	2.1	6.4	1.1

The parameters for the chain defect motion were kept constant (ρ is 0.1, i.e., 0.9 kink/chain); r_2 is 7.5 $\times 10^{10}$ s^{-1}). L is the height of the cylinder and thus double the diffusion amplitude, R is its radius, and $D_\parallel$ ($D_\perp$) are the diffusion constants parallel (perpendicular) to the cylinder axis. The errors given in the first line are typical for all measurements.

To keep the number of fitting parameters as small as possible, the parameters of the kink motion were kept constant at values extrapolated for the gel phase close to the transition ($\rho = 0.1$, i.e., 0.9 kink/chain; r_2 is 7.5×10^{10} s^{-1}). With this procedure, we can obtain an *upper limit* of the diffusion inside the solvation cage, as we most probably underestimate the chain motion.

The result is shown in Table 3. Parameters for the motion in the plane of the membrane ($D_\perp$, R) were obtained from measurements in the 135° orientation; parameters for the out-of-plane motion ($D_\parallel$, L), from the 45° orientation. It should be noted that the process of diffusion in a solvation cage starts already a little below T_c. This is easily comprehensible, as the phase transition in this low hydration region extends over several degrees and thus starts already at temperatures below T_c.

It can be seen that the diffusion constants depend strongly on the reduced temperature, i.e., the temperature difference to the phase transition. The height of the cylinder depends on both the temperature and hydration: the lower the hydration, the smaller the cylinder.

DISCUSSION

Träuble (1971) put forward the idea of a kink diffusing along the chain as a reason for unspecific transport of small molecules through the membrane, which is observed experimentally. From the water permeability of membranes he calculated the diffusion coefficient for kinks. He predicted a rate of 5×10^{10} s^{-1}, which was also found in molecular dynamics simulations (Egberts and Berendsen, 1988). Our values for the jump rates of a kink in the gel phase lie in the range of $6–10 \times 10^{10}$ s^{-1} and thus agree well with the predictions.

In the liquid crystalline phase the model of one chain defect is not sufficient to describe the spectra taken. Therefore an additional, local diffusion inside a cylinder (representing the solvation cage) is assumed. The most interesting aspect of the present study is the motion parallel to the membrane normal (or out-of-plane motion), as such motion has been discussed rather controversial in past years (Rand and Parsegian, 1989; Israelschvilli and Wennerstroem, 1992). This out-of-plane motion can have two contributions: an individual diffusion of each molecule, uncorrelated with the motion of its neighbors, or a collective undulation motion of the membrane. Inasmuch as incoherent scattering cannot distinguish correlated and uncorrelated motions, we will discuss both contributions.

The collective motion of a membrane can have several modes. The mode that should contribute most to the high-frequency window of the TOF measurements is the bending mode (Helfrich and Servuss, 1984, deGennes, 1974):

$$\Gamma = \frac{K_c}{d\eta} q^2, \tag{11}$$

where K_c is the bending elasticity, η is the effective viscosity of the lipid-water system (dominated by the water viscosity), and d is the repeat distance of the multilayers.

While the wave vector q lies in the plane of the membrane, the amplitude u of the mode is parallel to the membrane normal. DeGennes (1974) calculated this amplitude to be

$$\langle u^2 \rangle = \frac{kT}{AK_c q^4}, \tag{12}$$

where $\langle u^2 \rangle$ is the mean value of the amplitude squared, kT is the thermal energy, and A is the undulating area.

As incoherent neutron scattering is not mode selective, one has to integrate over all modes that lie in the observed frequency window. The total amplitude is then a sum over the corresponding amplitudes, which can be written as follows:

$$\langle u_{\text{eff}}^2 \rangle = \sum_q \langle u^2 \rangle \rightarrow \frac{\Delta}{2\pi} \int \frac{kT}{AK_c q^4} q \mathrm{d}q. \tag{13}$$

Using the dispersion relation [eq. 11], one obtains

$$\langle u_{\text{eff}}^2 \rangle = \frac{kT}{4\pi d\eta} \int_{\Gamma_{\min}}^{\Gamma_{\max}} \frac{1}{\Gamma^2} \mathrm{d}\Gamma \approx \frac{kT}{4\pi d\eta} \frac{1}{\Gamma_{\min}}. \tag{14}$$

As the minimum and maximum frequencies differ by a factor of about 20, we can neglect the upper boundary in first approximation. For a resolution of 25 μeV (as obtained on MIBEMOL), this leads to $\langle u_{\text{eff}}^2 \rangle = 0.1$ Å^2, i.e., an amplitude much smaller than observed experimentally. In summary, the above considerations show that the classical bending mode cannot explain the time-of-flight data. However, for the much slower time scale measured at the backscattering spectrometer (König et al., 1992), the estimated amplitude for the bending mode is $\langle u_{\text{eff}}^2 \rangle = 4.0$ Å^2, which agrees well with the experimental data.

If we now discuss the other possible motion to explain our measured amplitudes, i.e., protrusion of single molecules, and consider all lipids to be at the same vertical position, an amplitude of 1–1.5 Å corresponds to the exposure of 0.8–1.2 CH_2 groups to water. The time scale that corresponds to protrusion at a given length scale has been calculated for micelles by Aniansson (1978). Taking his results, we can estimate a time scale of 3×10^{-11} s for the protrusion of one CH_2 group, which corresponds well with the time scale of time-of-flight measurements. From the critical micelle concentration, the energy per length needed to expose hydrocarbon chains to water has been estimated (e.g., Israelachvilli, 1992) to be $\alpha_p = 5–6 \times 10^{-21}$ J/m. Taking the thermal energy corresponding to our experimental conditions, we obtain $\alpha_p = 3–5 \times 10^{-21}$ J/m, i.e., a slightly lower value. However, the critical micelle concentration model does not take into account neither bilayer geometry or lipid packing parameters, and thus our experiments could contribute to a more realistic model. In a recent theoretical paper on the interplay of hydration (i.e., forces that are due to a disturbance of solvent structure) and protrusion forces (i.e., forces that are due to out-of-plane motion of the membrane molecules) by Lipowsky and Grotehans (1993), it is shown that both mechanisms contribute to a strong short-range

repulsion. If protrusion interactions dominate, the authors estimate a decay length of ~1 Å (including both protrusions of single molecules and correlated displacements of several molecules). On the other hand, if hydration forces dominate (i.e., the protrusions have a very small amplitude), the decay length of the resulting force will be dominated by solvent properties (Marcelja and Radic, 1976). In general it is not easy to distinguish the two possible mechanisms by a simple measurement of the decay length alone.

Our measurements show that there is a protrusion interaction in the liquid crystalline phase with amplitudes of 1–1.5 Å, but not in the gel phase. Comparing the calculated orders of magnitudes and the experimental results, one should consider the possibility that the dominating interaction for the short range repulsion is actually different in the two phases. To verify this hypothesis, temperature-dependent force measurements should be carried out, as Lipowsky and Grotehans (1993) suggest a different temperature dependence for the two mechanisms.

In a recent paper on water dynamics (König et al., 1993) the out-of-plane motion described here for low hydration could not be observed for the water, and this seems to be a contradiction at first sight. However, after a closer look, the water dynamics for the bound water using quasi-elastic neutron scattering was determined mainly in the gel phase, and the lack of an out-of-plane motion in this phase is in agreement with our results on lipid motion. Only one measurement on bound water was performed in the liquid crystalline phase, and its resolution was not sufficient to identify clearly another motion additional to the internal water motion observed.

CONCLUSION

The hydration dependence of local diffusion as well as of chain motions of DPPC molecules is studied in the gel and liquid crystalline phases. In the gel phase it is sufficient to consider the dynamics of a chain defect as an explanation of the experimental spectra. Deriving the scattering functions for two simplified cases of chain defects and comparing them justified the use of a rather simple model for the fitting procedure. However, in the liquid crystalline phase the spectra cannot be explained by chain dynamics alone, and an additional motion, the diffusion of the molecule in its solvation cage, has to be assumed. Thereby an upper limit for the amplitude of protrusion for the DPPC molecules can be measured directly and is determined to be 1–1.5 Å, depending on temperature and hydration.

APPENDIX

In going from an-all *trans* configuration of a chain to one with a kink, one has to consider the different jump lengths involved. The lengths mentioned already in the text will be presented here.

In Fig. 5 a chain in the all-*trans* configuration is depicted. If a kink is created at position 2 (sketch in the middle), the proton at position 2 rotates around the C—C bond and thus changes its orientation with respect to the chain (d_1). The proton at position 3 experiences a translation as well as a change of orientation (d_2); positions 4 to the end of the chain are only translated (d_3).

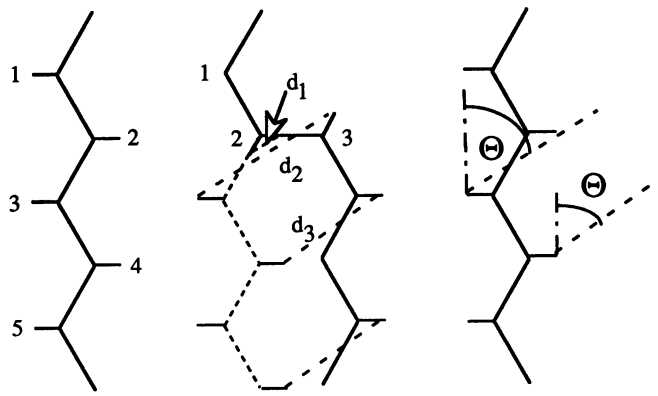

FIGURE 5 Chain geometry for an all-*trans* configuration (*left*) and one kink defect (*middle*). The indicated lengths d_1, d_2 and d_3 show the jump lengths involved. The sketch to the *right* shows the angle Θ between jump axis and membrane normal.

Taking the C—C bond length to be 1.54 Å, the C—H bond length to be 1.1 Å, and a bond angle of 120° leads to d_1 = 1.65 Å, d_2 = 3.9, Å, d_3 = 2.25 Å.

As the jump vector **d** is not parallel or perpendicular to the membrane normal **n** but encloses an angle Θ with **n**, this angle has to be taken into account when analyzing the different orientations of the sample with the neutron beam. The sketch to the right in Fig. 5 shows this angle Θ as used in the text.

We thank Dr. A. Fleischmann for his help with the measurements at the reactor of the TU Munich in Garching.

The work was funded by a grant of the German Ministry of Research and Technology (BMFT project 03SATUM-2).

REFERENCES

Aniansson, G. E. A. 1978. Dynamics and structure of micelles and other amphiphile structures. *J. Phys. Chem.* 82:2805–2808.

Bahar, I., and B. Erman. 1987. Investigations of local motions in polymers by the dynamic rotational isomeric state model. *Macromolecules.* 20: 1368–1376.

Barnes, J. D. 1973. Inelastic neutron scattering study of the "rotator" phase transition in *n*-nonadecans. *J. Chem. Phys.* 50:5193–5201.

Bée, M. 1988. Quasielastic Neutron Scattering. Adam Hilger, Bristol, UK.

Blume, A. 1993. Combination of FT-IR and 2H-NMR spectroscopy for the study of structure and dynamics in membranes. Presented at meeting on membrane structure, dynamics and interactions via neutron and x-ray scattering. Saclay, France, April 1993.

Caillé, A., D. Pink, F. de Vertouil, and M. Zuckermann. 1980. Theoretical models for quasi-two-dimensional mesomorphic monolayers and membrane bilayers. *Can. J. Phys.* 58:581–586.

Casal, H. L., and R. N. McElhaney. 1990. Quantitative determination of hydrocarbon chain conformational order in bilayers of saturated phosphatidylcholines of various lengths. *Biochemistry.* 29:5423–5427.

deGennes, P. G. 1974. The Physics of Liquid Crystals. Clarendon Press, Oxford, UK.

Dianoux, A. J., M. Pineri, and F. Volino. 1982. Neutron incoherent scattering law for restricted diffusion inside a volume with an anisotropic shape. Application to the problem of water absorbed in naflon membranes. *Mol. Phys.* 46:129–137.

Dolainsky, C., A. Möps, and T. M. Bayerl. 1993. Transverse relaxation in supported and nonsupported phospholipid model membranes and the influence of ultraslow motions: a ^{31}P-NMR study. *J. Chem. Phys.* 98:1712–1720.

Egberts, E., and H. J. C. Berendsen. 1988. Molecular dynamics simulation of a smectic liquid crystal with atomic detail. *J. Chem. Phys.* 89:3718–3732.

Galla, H. J., W. Hartmann, U. Theilen, and E. Sackmann. 1979. On two-dimensional passive random walk in lipid bilayers and fluid pathways in biomembranes. *J. Membr. Biol.* 48:215–236.

Hauser, H., L. Pascher, R. H. Pearson, and S. Sundell. 1981. Preferred conformation and molecular packing of phosphatidylethanolamine and phosphatidylcholine. *Biochim. Biophys. Acta.* 650:21–51.

Helfand, E., and J. Skolnick. 1982. Mechanism and rates of conformational transitions in heterogeneous polymers. *J. Chem. Phys.* 77:5714–5724.

Helfrich, W., and R.-M. Servuss. 1984. Undulations, steric interaction and cohesion of fluid membranes. *Nuovo Cimento.* 3D:137–151.

Israelachvilli, J. 1992. *Intermolecular and Surface Forces*, 2nd ed. Academic Press, San Diego, CA.

Israelachvilli, J. N., and H. Wennerstroem. 1992. Entropic forces between amphiphilic surfaces in liquids. *J. Phys. Chem.* 96:520–531.

Jürgens, E. 1981. Untersuchungen zur Lipid-Wasser-Wechselwirkung in ungeordneten und makroskopisch orientierten Modellmembranen. Ph.D. thesis. Universität Ulm, Ulm, Germany.

Koechy, T., and T. M. Bayerl. 1993. Lateral diffusion coefficients of phospholipids in spherical bilayers on a solid support measured by 2H-nuclear-magnetic-resonance relaxation. *Phys. Rev. E.* 47:2109–2116.

König, S., W. Pfeiffer, T. Bayerl, D. Richter, and E. Sackmann. 1992. Molecular dynamics of lipid bilayers studied by incoherent quasi-elastic neutron scattering. *J. Phys. II* 2:1589–1615.

König, S., E. Sackmann, D. Richter, R. Zorn, C. J. Carlile, and T. Bayerl. 1994. Molecular dynamics of water in oriented DPPC multilayers studied by quasielastic neutron scattering and deuterium-NMR relaxation. *J. Chem. Phys.* 100:3307–3316.

Levine, Y. K., A. I. Bailey, and M. H. Wilkins. 1968. Multilayers of phospholipid bimolecular leaflets. *Nature.* 220:577–578.

Lipowsky, R., and S. Grotehans. 1993. Hydration vs protrusion forces between lipid bilayers. *Europhys. Lett.* 23:599–604.

Lovesey, S. W. 1984. Theory of Neutron Scattering from Condensed Matter. Oxford University Press, Oxford, UK.

Marcelja, S., and N. Radic. 1976. Repulsion of surfaces due to boundary water. *Chem. Phys. Lett.* 42:129–130.

Mayer, C., K. Müller, K. Weisz, and G. Kothe. 1988. Deuteron NMR relaxation studies of phospholipid membranes. *Liq. Cryst.* 3:797–810.

Mendelssohn, R., M. A. Davies, J. W. Brauner, H. F. Schuster, and R. A. Dluhy. 1989. Conformational disorder in the acyl chains of phospholipid bilayers by infrared spectroscopy. *Biochemistry* 28:8934–8939.

Mouritson, O. G., and M. Bloom. 1993. Models of lipid-protein interactions in membranes. *Ann. Rev. Biophys. Biomol. Struct.* 22:145–171.

Peters, R., and K. Beck. 1983. Translational diffusion in phospholipid monolayers measured by fluorescence microphotolysis. *Proc. Nat. Acad. Sci. USA.* 80: p. 7183–7187.

Pfeiffer, W., T. Henkel, E. Sackmann, W. Knoll, and D. Richter. 1989. Local dynamics of lipid bilayers studied by incoherent quasielastic neutron scattering. *Europhys. Lett.* 8:201–206.

Rand, R. P., and V. A. Parsegian. 1989. Hydration force between phospholipid bilayers. *Biochim. Biophys. Acta.* 988:351–376.

Richter, D., and Ewen, B. 1978. Non-periodic molecular motions in the modifications C and D of uniaxially oriented n-$C_{33}H_{68}$. In *Neutron Inelastic Scattering 1977.* International Atomic Energy Agency, Vienna.

Sackmann, E. 1983. Physical foundations of the molecular organization and dynamics of membranes. In Biophysics. W. Hoppe, editor. Springer-Verlag, Berlin.

Schindler, H., and J. Seelig. 1975. Deuterium order parameters in relation to thermodynamic properties of a phospholipid bilayer. A statistical mechanical interpretation. *Biochemistry.* 14:2283–2287.

Smith, J. 1991. Protein dynamics: comparison of simulations with inelastic neutron scattering experiments. *Q. Rev. Biophys.* 24:227–291.

Springer, T. 1972. Quasielastic Neutron Scattering for the Investigation of Diffusive Motions in Solids and Liquids. Vol. 64 of Springer Tracts in Modern Physics. Springer-Verlag, Berlin.

Tabony, J., and Perly, B. 1990. Quasielastic neutron scattering measurements of fast local translational diffusion of lipid molecules in phospholipid bilayers. *Biochim. Biophys. Acta.* 1063:67–72.

Tardieu, A., and V. Luzzaki. 1973. Structure and polymorphism of the hydrocarbon chains of lipids: a study of lecithin-water phases. *J. Mol. Biol.* 75:711–733.

Torbet, J., and M. H. F. Wilkins. 1976. X-ray diffraction of lecithin bilayers. *J. Theor. Biol.* 62:447–458.

Träuble, H. 1971. The movement of molecules across lipid membranes: a molecular theory. *J. Membr. Biol.* 4:193–208.

Vaz, W. L. C., R. M. Clegg, and D. Hallmann. 1985. Translational diffusion of lipids in liquid crystalline phase phosphatidylcholine multibilayers. A comparison of experiment with theory. *Biochemistry.* 24:781–786.